Jpn. J. Appl. Phys. Vol. 39 (2000) pp. 1656–1659
Part 1, No. 4A, April 2000

Improvement of Electrical Properties of Pulsed Laser Crystallized Silicon Films by Oxygen Plasma Treatment

Yoshiyuki TSUNODA, Toshiyuki SAMESHIMA and Seiichiro HIGASHI[1]

Tokyo University of Agriculture and Technology, 2-24-16 Nakamachi, Koganei, Tokyo 184-8588, Japan
[1]*SEIKO EPSON Corporation, Nagano 392-8502, Japan*

(Received October 27, 1999; accepted for publication January 19, 2000)

Changes in the electrical properties of pulsed laser crystallized silicon films with oxygen plasma treatment were investigated. 50-nm-thick silicon films doped with $7.4 \times 10^{17}\,cm^{-3}$ phosphorus atoms crystallized by a 308-nm-XeCl excimer laser at an energy density of $400\,mJ/cm^2$ were treated by 30-W-RF plasma of oxygen gas at 130 Pa at 250°C. The electrical conductivity markedly increased from 6.9×10^{-5} S/cm (as crystallized) to 10 S/cm by heat treatment for 40 min. Theoretical analysis of the electrical conductivity revealed that the potential barrier height at grain boundaries decreased from 0.32 eV (as crystallized) to almost zero, and that carrier mobility increased from $15\,cm^2/Vs$ (as crystallized) to $170\,cm^2/Vs$.

KEYWORDS: LPCVD, polycrystalline silicon, laser crystallization, excimer laser, carrier density, carrier mobility, activation energy, potential barrier height, oxidation

1. Introduction

Formation of polycrystalline silicon films by pulsed laser annealing is attractive for low temperature fabrication processes because crystallization occurs rapidly and no thermal damage is induced in the glass substrates.[1–3] This is advantageous for the fabrication of devices such as polycrystalline silicon thin film transistors (poly-Si TFTs) at low temperatures. However rapid and local heating using pulsed laser can cause a large number of defect states in laser crystallized silicon films. To overcome this problem, many investigations using hydrogenation have been reported.[4–10]

In this paper, we report the passivation phenomena of grain boundaries of laser crystallized silicon films by oxygen plasma treatment. We present changes in the electrical properties of laser crystallized lightly doped silicon films associated with the reduction of the density of defect states by oxygen plasma treatment. Increases in the carrier density and the carrier mobility are reported. Reduction of the potential barrier height at grain boundaries is also discussed. Moreover, thermal stability in the electrical conductivity is discussed.

2. Experimental

Amorphous silicon films of 50 nm thickness were formed by chemical vapor deposition (LPCVD) on quartz substrates at 425°C. $7.4 \times 10^{17}\,cm^{-3}$-phosphorus atoms were implanted into the silicon films by ion implantation. Al electrodes with a gap of 400 μm and a width of 2000 μm were formed on the silicon surface. Samples were irradiated in vacuum at 10^{-4} Pa at 250°C by a 28-ns pulsed XeCl excimer laser through a quartz window. Multistep-laser irradiation was carried out. The laser energy density was increased from $160\,mJ/cm^2$ (crystallization threshold) to $400\,mJ/cm^2$ in $20\,mJ/cm^2$ steps. Five pulses were irradiated at each laser energy density step. Immediately after the crystallization, oxygen gasses at 100 sccm was introduced under a pressure of 130 Pa in the chamber and one of the electrodes was positioned in front of the samples, then oxygen plasma at 30 W was generated by applying radio frequency voltages to the electrode.

3. Results and Discussion

Figure 1 shows the electrical conductivity as a function of the duration of oxygen plasma treatment for samples crystallized at laser energy densities of $240\,mJ/cm^2$, $340\,mJ/cm^2$ and $400\,mJ/cm^2$, respectively. As-crystallized films had very low electrical conductivities of 10^{-4}–10^{-6} S/cm. This indicates that there was a low density of free carriers in the films although it has been believed that all phosphorus atoms are placed in substitutional silicon lattice sites through pulsed laser rapid melt regrowth.[11,12] On the other hand, the electrical conductivity markedly increased as the duration of oxygen plasma treatment increased for every sample. For samples crystallized at $400\,mJ/cm^2$, the electrical conductivity increased from 6.9×10^{-5} S/cm to 10 S/cm by oxygen plasma treatment for 40 min. This clearly shows that the free carrier density increased through oxygen plasma treatment for the $7.4 \times 10^{17}\,cm^{-3}$ phosphorus doping case.

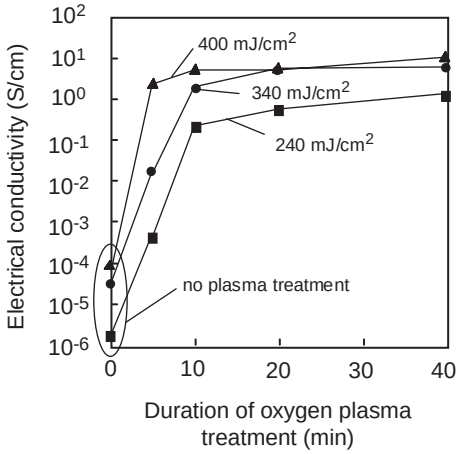

Fig. 1. Electrical conductivity as a function of the duration of oxygen plasma treatment at 30 W and at 250°C for $7.4 \times 10^{17}\,cm^{-3}$-phosphorus -doped silicon films 50 nm thick crystallized at laser energy densities of 240, 340 and $400\,mJ/cm^2$ respectively. The electrical conductivity for as-crystallized films is also shown. Solid curves are guide for the eyes.

Figure 2 shows the electrical conductivity as a reciprocal function of absolute temperature with different plasma durations for the $400\,mJ/cm^2$ crystallization case. Before oxygen plasma treatment, the electrical conductivity rapidly increased with an activation energy of 0.4 eV as the temperature increased. The temperature dependence indicates that the Fermi level was located near the mid gap region for as-

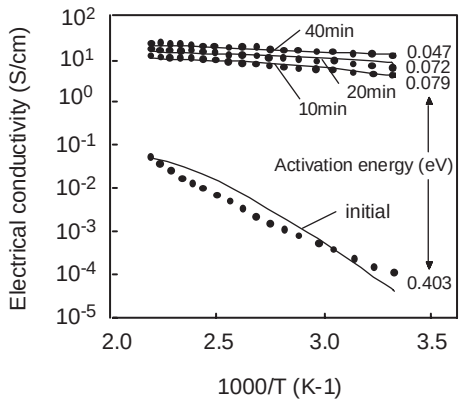

Fig. 2. Temperature dependence of the electrical conductivity for 7.4×10^{17} cm^{-3}-phosphorus doped silicon films 50-nm-thick crystallized at 400 mJ/cm^2 treated with different plasma durations and as crystallized (solid circles). Activation energy is presented for each fabrication condition. Solid curves indicate electrical conductivities calculated under the conditions of 7.4×10^{17} cm^{-3} phosphorus doping, defect states with an energy level of 0.12 eV above the mid gap and a width of 0.3 eV, an average grain size of 55 nm and an oxygen diffusion coefficient of 1.1×10^{-14} cm^2/s. The energy level and width of defect states, and the oxygen diffusion coefficient were analytically determined by the fitting process between experimental and calculated electrical conductivities.

crystallized silicon films. After oxygen plasma treatment, the electrical conductivity increased and the activation energy decreased as shown in Fig. 2.

According to our recent study using ESR measurements,[12] pulsed laser crystallized films had a high density of dangling bond electrons of about 10^{18} cm^{-3}, which were localized at grain boundaries.[13–17] The defects caused by the dangling bonds trapped most of the free electrons generated from ionized phosphorus atoms so that silicon films had the depletion states with a low conductivity. From the results of Figs. 1 and 2, oxygen plasma treatment made the defects electrically inactive and changed the localized electron states to extended states. Defect states localized at grain boundaries for laser-crystallized silicon films would be oxidized by oxygen atoms incorporated into silicon films with the help of heating energy. The dangling bonds of silicon atoms were eliminated and Si–O bondings were formed.

In order to understand changes in the electrical conductivity of polycrystalline films, we developed a statistical thermodynamical analysis program.[14,17,18] We introduced a Gaussian-type energy distribution of density of defect states in the band gap whose energy level at the maximum density and the width can be changed. Phosphorus dopant atoms were assumed to be distributed uniformly in silicon films. Electron carriers are generated from the phosphorus dopant atoms via their ionization, whose probability is determined with the Fermi-Dirac statistical distribution function. Free carriers are trapped by the localized defect states and the defects are charged negatively. The Fermi energy level and the free carrier density at the midpoint of crystalline grains are determined by the statistical thermodynamical conditions keeping the charge neutrality among the densities of ionized dopant atoms N_d, and the defect states charged negatively with electron carriers (X_d) and free carriers (n) ($N_\mathrm{d} = n + X_\mathrm{d}$) in the entire region including crystalline grains and grain boundaries. However, the density of ionized donors is larger than that of free electron in crystalline grains because some electrons produced from doped phosphorus atoms are trapped at grain boundaries, although the charge neutrality is always established in the entire semiconductor region. This space charge effect in crystalline grains causes band bending and results in the potential barrier at grain boundaries, which is determined by the difference in potential at the conduction band edge between the midpoint of crystalline grains and their boundaries. The potential energy, $\phi(x)$, at x, which is the distance from midpoint of the crystalline grain is calculated using the Poisson equation with the density of space charges ($N_\mathrm{d} - n$) as

$$\frac{\partial^2 \phi(x)}{\partial x^2} = \frac{e(N_\mathrm{d} - n)}{\epsilon_\mathrm{s}\epsilon_\mathrm{o}}, \tag{1}$$

where e is the elemental charge, ϵ_o is the vacuum dielectric constant and ϵ_s is the dielectric permittivity of silicon. The Fermi energy level is determined using Boltzmann thermodynamical statistics while maintaining the charge neutrality condition over the entire region.

The carrier density $n(x)$ at point x in the lateral direction from the midpoint of the crystalline grain is given as

$$n(x) = N_\mathrm{c} \exp\left(\frac{-e(E_\mathrm{g} - E_\mathrm{f} + \phi(x))}{kT}\right), \tag{2}$$

where N_c is the effective density of states at the conduction band edge, E_g is the energy band gap, E_f is the height of the Fermi level from the valence band edge at the midpoint of the crystalline grains, k is the Boltzmann constant and T is the absolute temperature. The effective carrier density in the lateral direction was calculated because the band bending causes a distribution of the free carrier density in the lateral direction. The carrier density in the lateral direction, n_lateral, is obtained from integration of the reciprocal number of carrier density from the midpoint to the grain boundary as,

$$n_\mathrm{lateral} = \left(\frac{2}{L}\int_0^{\frac{L}{2}} \frac{1}{n(x)} dx\right)^{-1}, \tag{3}$$

where L is the average crystalline grain size. If there is a high potential barrier at grain boundaries, the carrier density is very low at the boundaries, so that the effective carrier density in the lateral direction becomes much lower than that of the average free carrier density in crystalline grains.

Oxygen plasma treatment was included in the analysis program by the assumption that oxygen atoms were incorporated into the films with a diffusion constant. The oxygen flux distributes according to the complementary error function. The density of the defect states at a given film depth is assumed to be reduced in proportion to the reaction probability and the density of oxygen atoms according to the following equation.

$$\frac{dn_\mathrm{d}}{dt} = -pt, \tag{4}$$

$$F = F_0 \,\mathrm{erft}\,\frac{x}{2\sqrt{Dt}}, \tag{5}$$

where n_d is the density of defect states, p is the reaction probability, F_0 is the oxygen flux entering silicon films and D is the diffusion coefficient of oxygen atoms into silicon films. We also introduce scattering effects due to dopant ions, lattice vibration and disordered states at grain boundaries, which reduces the carrier mobility. We used the carrier scattering effect of dopant ions and lattice vibration reported by Irvin[19] and Prince,[20] while the mobility reduction rate due to

lattice disordered states was determined by a fitting process between experimental and calculated results. The effective electrical conductivity was obtained with the calculation program described above. Through the fitting process between temperature dependences of calculated and experimental conductivities for the initial as-crystallized case shown in Fig. 2, energy level and its width for defect states were determined as 0.12 eV above the mid gap and 0.3 eV, respectively. Then the oxygen flux × the reaction probability and the oxygen diffusion coefficient were obtained by fitting the activation energies of the calculated electrical conductivity to the experimental values for every temperature and every duration of plasma treatment as shown in Fig. 2. Values of oxygen flux × reaction probability, pF_0, and the oxygen diffusion coefficient, D, shown in eq. (4) were determined to be $6.6 \times 10^{16}\,\mathrm{cm^{-3}/s}$ and $1.1 \times 10^{-14}\,\mathrm{cm^2/s}$, respectively. Finally the mobility reduction rate due to scattering at grain boundaries (0–1) was determined by the agreement between experimental and calculated conductivities for every temperature and every duration of plasma treatment. The mobility reduction rate gives the carrier mobility.

Figure 3 shows the average free carrier density existing in crystalline grains and the effective carrier density in the lateral direction at room temperature, which were obtained for the case of crystallization at $400\,\mathrm{mJ/cm^2}$. Although the as-crystallized films had a rather high average free carrier density $\sim 10^{17}\,\mathrm{cm^{-3}}$ in crystalline grains, the effective carrier density in the lateral direction was very low, $2 \times 10^{13}\,\mathrm{cm^{-3}}$, because the high potential barrier at grain boundaries blocked carrier transfer. Oxygen plasma treatment increased both carrier densities. The effective carrier density in the lateral direction became similar to the average carrier density in crystalline grains because the plasma treatment reduced the defect density and the potential barrier height, as shown in Fig. 3. For the as-crystallized case at $400\,\mathrm{mJ/cm^2}$, the potential barrier was very high, 0.32 eV, caused by $4 \times 10^{17}\,\mathrm{cm^{-3}}$-defect states trapping free electrons. The potential barrier height was reduced to almost zero according to the reduction of the density of defect states lower than $1 \times 10^{17}\,\mathrm{cm^{-3}}$ by oxygen plasma treatment longer than 20 min, as shown in Fig. 4. The change in the carrier mobility as a function of the duration of oxygen plasma treatment was also estimated for the $400\,\mathrm{mJ/cm^2}$-crystallization case, as shown in Fig. 5. The mobility was low at $15\,\mathrm{cm^2/Vs}$ because of a high carrier scattering at grain boundaries for as-crystallized films. It increased to $170\,\mathrm{cm^2/Vs}$ as the oxygen plasma duration increased to 40 min. This result indicates that the oxidation of grain boundaries may reduce the carrier scattering effect and realize a good carrier transfer probability.

The density of defect states was also estimated to be 1.1×10^{18} and $6 \times 10^{17}\,\mathrm{cm^{-3}}$ for as-crystallized films at 240 and $340\,\mathrm{mJ/cm^2}$ respectively, which were higher than that for the $400\,\mathrm{mJ/cm^2}$ crystallization case. The experimental results and theoretical analysis show that the oxygen atoms effectively terminated defect states below $10^{17}\,\mathrm{cm^{-3}}$ for 40-min-plasma treatments. High conductivity after plasma treatments suggested that grain boundaries had high carrier transfer characteristics and no substantial insulating SiO_2 region was formed, probably because the duration of plasma treatment was too short to form the SiO_2 region through oxidization of silicon with oxygen atoms throughout 50-nm-thick films at 250°C.

In order to investigate the thermal stability of oxygen

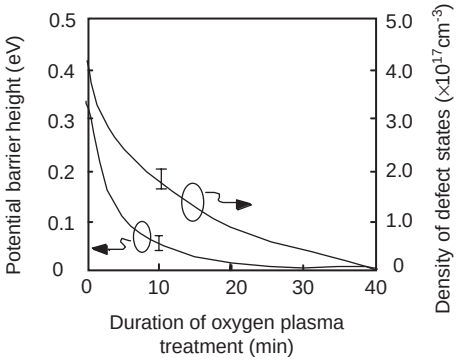

Fig. 4. Potential barrier height at grain boundaries and density of defect states calculated with the conditions given in Fig. 2 as functions of oxygen plasma treatment duration for the 400-mJ/cm^2-crystallization case. The error bars indicate the region of the potential barrier height and the density of defect states giving the best fitting.

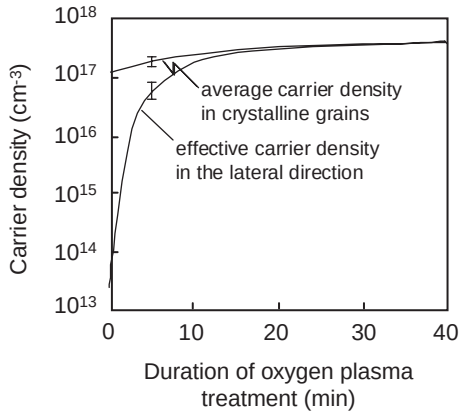

Fig. 3. Average carrier density in crystalline grains and effective carrier density in the lateral direction as functions of oxygen plasma treatment duration for the 400-mJ/cm^2-crystallization case. The carrier densities were obtained through a fitting process between experimental and calculated electrical conductivities given in Fig. 2. The error bar presents the region of the carrier density giving the best fitting.

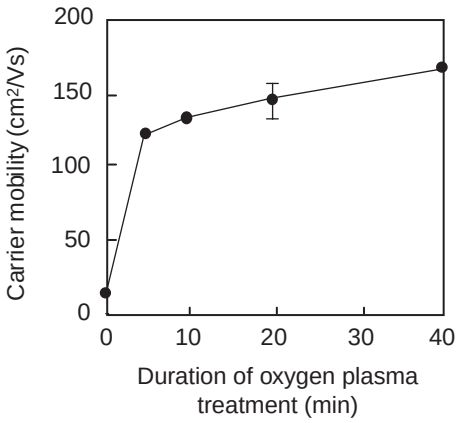

Fig. 5. Electron carrier mobility estimated using calculations with the conditions given in Fig. 2 as a function of oxygen plasma treatment duration for the 400-mJ/cm^2-crystallization case. The mobility was determined by giving the mobility redution rate at grain boundaries, where calculated conductivities agreed well with experimental ones. The error bar indicates the region of the carrier mobility giving the best fitting.

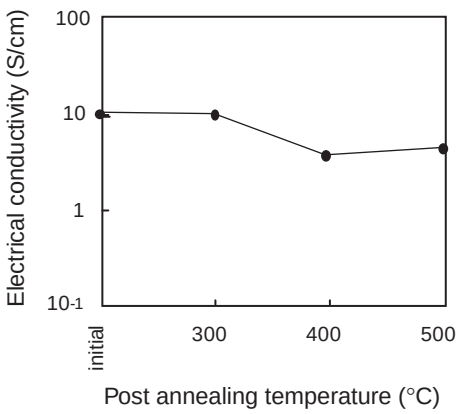

Fig. 6. Electrical conductivity as a function of temperature of post annealing for 1 h for samples crystallized at 400 mJ/cm^2 treated with oxygen plasma at 250°C for 40 min at 30 W at oxygen gas pressure 130 Pa. The solid curve is a guide for the eyes.

plasma passivation, we measured the change in the electrical conductivity for samples crystallized at 400 mJ/cm^2 treated with oxygen plasma at 250°C for 40 min at 30 W at an oxygen gas pressure of 130 Pa when the samples were heated up to 500°C for 1 h in air. The electrical conductivity slightly decreased from 10 to 5 S/cm as the heating temperature increased to 500°C, as shown in Fig. 6. This result indicates that defects which can trap free carriers were not seriously increased by 500°C post annealing and oxygen termination of silicon dangling bonds was rather stable. Oxygen plasma treatment will be useful for grain boundary passivation at low temperatures. Thermally stable characteristics of the electrical conductivity might result in stable characteristics of TFTs operated in high electric stress fields.

4. Summary

We investigated the change in the electrical properties of laser crystallized 7.4×10^{17} cm^{-3}-phosphorus doped silicon films with oxygen plasma treatment. RF oxygen plasma treatment for 40 min at 30 W at 130 Pa increased the electrical conductivity from 6.9×10^{-5} S/cm (as crystallized) to 10 S/cm. Our numerical analysis of electrical conductivities revealed that the density of defect states was reduced from 4×10^{17} cm^{-3} (initial) to lower than 1×10^{17} cm^{-3}. The potential barrier height was reduced from 0.32 eV (initial) to almost zero. These reductions markedly increased the effective carrier density in the lateral direction. The oxygen plasma treatment oxidized the dangling bonds of silicon at grain boundaries and made them electrically inactive. Oxygen plasma treatment also resulted in an increase of the carrier mobility of 170 cm^2/Vs. No serious decrease of the electrical conductivity was observed after post annealing up to 500°C. These experimental and theoretical results indicate that oxygen plasma treatment is useful for improvement of the electrical properties of laser-crystallized silicon films.

Acknowledgements

We thank Professors. T.Saitoh and T.Mohri for their support.

1) T. Sameshima, M. Hara and S. Usui: Jpn. J. Appl. Phys. **29** (1990) L548.
2) T. Sameshima and S. Usui: J. Appl. Phys. **70** (1991) 1281.
3) T. Sameshima and S. Usui: J. Appl. Phys. **74** (1993) 6592.
4) K. Sera, F. Okumura, H. Uchida, S. Ito, S. Kaneko and K. Hotta: IEEE Trans. Electron Devices **36** (1989) 2868.
5) M. Rodder and S. Aur: IEEE Electron Device Lett. **12** (1991) 233.
6) R. A. Ditizio, G. Liu, S. J. Fonash, B. C. Hseih and D. W. Greve: Appl. Phys. Lett. **56** (1990) 1140.
7) T. Sameshima, M. Sekiya, M. Hara, N. Sano and A. Kohno: J. Appl. Phys. **76** (1994) 7377.
8) K. Baert, H. Murai, K. Kobayashi, H. Namizaki and M. Nunoshita: Jpn. J. Appl. Phys. **32** (1993) 2601.
9) I.-W. Wu, A. G. Lewis, T.-Y. Huang and A. Chiang: IEEE Electron Device Lett. **10** (1989) 123.
10) I. Yamamoto, H. Kuwano and Y. Saito: J. Appl. Phys. **71** (1992) 3350.
11) T. Sameshima, K. Saito, N. Aoyama, S. Higashi, M. Kondo and A. Matsuda: Jpn. J. Appl. Phys. **38** (1999) 1892.
12) T. Sameshima, S. Usui and H. Tomita: Jpn. J. Appl. Phys. **26** (1987) L1678.
13) S. Higashi, K. Ozaki, K. Sakamoto, Y. Kano and T. Sameshima: Jpn. J. Appl. Phys. **38** (1999) 857.
14) J. Y. W. Seto: J. Appl. Phys. **46** (1975) 5247.
15) W. B. Jachson, N. M. Joackson and D. K. Biegelsen: Appl. Phys. Lett. **43** (1983) 195.
16) C. H. Segar, G. E. Pike and D. S. Ginley: Phys. Rev. Lett. **43** (1979) 532.
17) K. Sakamoto, T. Sameshima, Y. Tsunoda and S. Higashi: Proc. Workshop on Active Matrix Liquid Crystal Displays, Tokyo, Japan, 1999, p. 131.
18) G. Baccarani and B. Ricco: J. Appl. Phys. **19** (1978) 5565.
19) J. C. Irvin: Bell Syst. Tech. J. **41** (1962) 387.
20) M. B. Prince: Phys. Rev. **94** (1954) 42.